Jurnal Teknologi

Full paper

Forced Cooling on a Heated Wall with Impinging Flow Configuration Using Synthetic Jet Actuator Under Combined Wave Excitation

Harinaldi*, Engkos A Kosasih, Damora Rhakasywi, Rikko Defriadi

[a]*Department of Mechanical Engineering, Faculty of Engineering, University of Indonesia - Kampus Baru UI Depok 16242*

*Corresponding author: harinald@eng.ui.ac.id

Article history

Received :15 June 2012
Received in revised form :12 August 2012
Accepted :28 August 2012

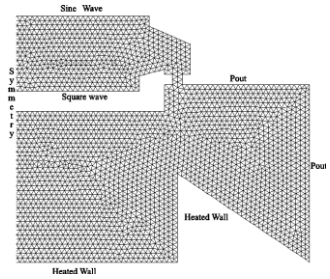

Abstract

This research investigated the forced cooling characterization of an impinging synthetic jet under combined wave excitation. The synthetic jet cooling used an air flowing in a vertical direction into the heated wall. The synthetic jet actuator used two oscilating membranes to push and pull the air from and to the cavity. The main purpose of this synthetic jet was to create vortices pair to come out from nozzle which will accelerate the heat transfer process occurring at the impinged wall. This heat transfer enhancement principles became the basis to simulate an alternative cooling system to substitute the conventional fan cooling in electronic devices application due to its advantage for having a small form factor and low noise. The investigation combined computational and experimental works. The model was simulated to examine the distribution of heat flow on the impinged walls using variation of turbulence model i.e. standard k-epsilon, realizable k-epsilon, standard k-omega and k-omega SST (Shear Stress Transport). Meshing order was elements tri and type pave and the number of grid was 4473 mesh faces to ensure detail discretization and more accurate calculation results. In the experiment the variation of sine and square wave signals were generated with sweep function generators to oscillate the membrane. The frequency of sine wave excitation for the first membrane was kept constant at 80 Hz, meanwhile the second membrane was excitated with varied square wave signals at 80 Hz, 120 Hz, and 160 Hz. Furthermore the velocity amplitude was 0.002 m/s. Some results indicate significant influence of the excitation, and combined waveform to the rate of heat transfer obtained.

Keywords: Heat transfer, synthetic jet, sine wave, square wave

1.0 INTRODUCTION

Efficient and effective cooling solutions are of big challange for the design of electronic devices to prevent thermal failure and to extend the working life of semiconductor components. In the new generation electronic devices, a good thermal management system is essential for reliable operation of integrated circuits since the heat dissipation is expected to be high due to high end processing and increase in frequency of operation. Generally heat sinks with different fin geometries and fan arrays are used for heat removal with air as a working fluid. However, fans require relatively large power to drive the flow because of narrow passages provided by the heat sinks.

The application of synthetic jet is a relatively new approach for electronics cooling. Synthetic jets operate on a simple principle, a flexible membrane forms one side of a partially enclosed chamber. Opposite to the membrane is an opening, such as an orifice. A mechanical actuator, piezoelectric diaphragm or magnetic coil causes the membrane to oscillate and periodically force air into and out of the opening. This results in a non-zero mean streamwise pulsating jet formed in front of the orifice which can be directed at a heated surface to enhance cooling. Harinaldi *et al*. (2011) have recently showed the potential of the originally designed synthetic jet actuator to reduced significantly the temperature of heated wall under impinged flow configuration. Chaudhari *et al*. (2009) showed that due to pulsating nature of the flow, the entrainment of ambient fluid into the jet was high as compared to that in a continuous jet, which supported effective cooling. Pavlova *et al*. (2006) have conducted experimental studies on impinging synthetic jets for constant heat flux surface cooling and compared its performance with a jet having no velocity fluctuations known as steady or continuous jet. They concluded that for the same Reynolds number, synthetic jets provide three times more effective cooling than the corresponding continuous jets. Gulati *et al*. (2009) discussed the effect of shape of nozzle on local heat transfer enhancement for different jet to plate spacings and Reynolds numbers. Amitay *et al*. (2006) experimentally investigated the efficiency and mechanism of cooling at constant heat flux surface by impinging synthetic jet. In the work a comparison with continuous jet was also presented. In their measurements, high frequency (1200 Hz) jets were found to be more effective at smaller axial distances and the low frequency (420 Hz) jets were found to be more effective at larger axial distances.

Chaudhari *et al*. (2010) apart from the above impingement studies, investigated the heat transfer characteristics of impinging

synthetic jet placed in a duct, for a certain electronic cooling (server/router) application. The heat transfer experiments included both direct impingement and cross-flow created using fan and another synthetic jet. Mahalingam *et al*. (2005) discussed the design and thermal performance of synthetic air-jet-based heat sink for high-power dissipation electronics. Approximately more than 40% of heat dissipation occurred with the synthetic jet-based heat sinks over the baseline configuration of steady air flow blown from a ducted fan through the heat sink. The average heat transfer coefficient in the channel flow between the fins was 2.5 times that obtained with steady flow in the duct at the same Reynolds number. Chaudhari *et al*. (2010) discussed the effect of different shapes of orifice on the heat transfer characteristics of synthetic jet. It was noticed that the rectangular orifice gives better heat transfer performance as compared to both square and circular orifice, at small axial distances. However, at large axial distances the square orifice out performed other orifice shapes investigated. Lee *et al*. (2004) studied the effect of nozzle diameter on impinging jet heat transfer and fluid flow. They reported that local Nusselt numbers in the region corresponding to $0 \leq r/d \leq 0.5$ increased with increasing nozzle diameter. Beitelmal *et al*. (2006) analyzed two-dimensional impinging jets and correlated heat transfers in the stagnation point, stagnation region and wall jet region with approximate solutions developed using simplified flow assumptions. Lienhard *et al*. (2006) analyzed heat transfer by impingement of circular free-surface liquid jets and analytical solutions were explained for heat transfer in different regions on the target plate.

Many prior studies were focused on the role of nozzle configuration on impingement heat transfer. Lee *et al*. (2000) studied the effect of nozzle configuration for l/d of 0.2 with three different types of profiles at nozzle exit, i.e., square edged, standard edged and sharp edged orifices. The tests were carried out for unconfined air jets impinging normally on smooth flat surface and the heat transfer results show that at stagnation region sharp edged orifice performs better. Tsubokura *et al*. (2002) used DNS to compute single-jet impingement from a nozzle with exit width of B and a spanwise dimension of πB. The influence of the spanwise period was investigated using simulations performed on a domain in which the spanwise dimension was increased to 5B. For this test, the solution was discretized using 54 grid points along this dimension in order to maintain the same grid spacing in the spanwise direction as in the baseline runs. Poh *et al*. (2005) conducted a numerical study of the heat transfer performance of a confined pulsed laminar impinging jet and showed that the spatial distribution of the time averaged Nusselt numbers become Reynolds number invariant in the laminar jet regime ($100 \leq Re \leq 1000$). Kercher *et al*. (2003) confirmed a power law relationship between Nu_0 and Re for an impinging synthetic jet, albeit for a limited range of Re and for an unspecified range of stroke lengths. The results showed the explicit dependence of Nu_0 on both Re and L_0, for a fixed jet-to-surface spacing H/D=2. Furthermore, Harinaldi *et al* (2011) conducted a synthetic jet simulation using CFD with Fluent software to show the characteristic heat transfer under triangular waveform by impinging synthetic jet.

In the present work a comprehensive study was done by computational and experimental method on an original design of synthetic jet actuator that operate based on membrane made of piezzo material. In the current stage, the main focus of the study was to characterize the temperature field of an impinging flow configuration with variation of membrane oscillation to generate turbulence flow. The purpose of using different functions on the double membrane is to create a continuous cooling process and keeps the fluid flow in a turbulent condition.

2.0 METHODS

2.1 Computational Approach

2.1.1 Meshing Development

The computational work was done to get the description of the flow and thermal field pattern of the impinging synthetic jet flow under periodical forcing. The modelling was conducted by using a commercial software Gambit 2.4.6®. This was done to provide meshing and boundary conditions for the simulation. The detail of the image is shown in Figure 1.

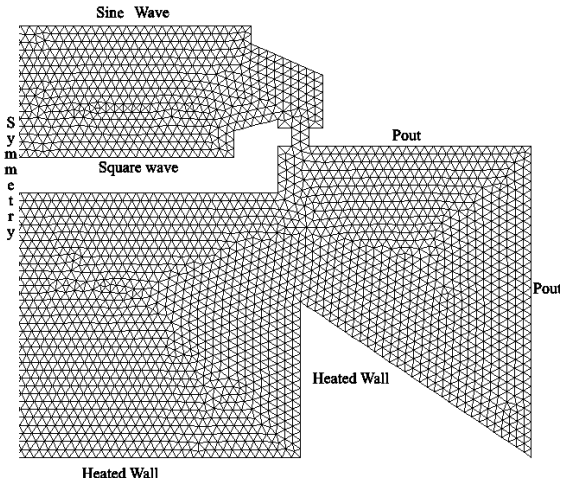

Figure 1 Computational Domain

The model used mesh type pave with element model tri and the number of meshing was about 4473 uniform mesh faces from top to bottom. The computational model was derived from an originally designed synthetic jet actuator configuration along with the heat sink as the heated wall. The simulation used fluent 6.3.26 ® for the computational solver.

2.1.2 Turbulence Model

Considering one of current objectives, the computational works investigate four turbulent model for simulation i.e standard k-ε, realizable k-ε, standard k- ω and k- ω SST (shear stress transport). Those turbulence model are further briefed in the following paragraphs.

The standard k-ε model is a semi-empirical model based on model transport equations for the turbulence kinetic energy (k) and its dissipation rate ε. The model transport equation for k is derived from the exact equation, while the model transport equation for ε was obtained using physical reasoning and bears little resemblance to its mathematical exact counterpart. In the derivation of the k-ε model, the assumption is that the flow is fully turbulent, and the effects of molecular viscosity are negligible. The transport equations for the Standard k-ε model are presented in Equations (1) and (2) :

$$\frac{\partial}{\partial t}(\rho k) + \frac{\partial}{\partial x_i}(\rho k u_i) = \frac{\partial}{\partial x_j}\left[\left(\mu + \frac{\mu_t}{\sigma_k}\right)\frac{\partial k}{\partial x_j}\right] + G_k + G_b - \rho\varepsilon - YM + S_k \quad (1)$$

$$\frac{\partial}{\partial t}(\rho \varepsilon) + \frac{\partial}{\partial x_i}(\rho \varepsilon u_i) = \frac{\partial}{\partial x_j}\left[\left(\mu + \frac{\mu_t}{\sigma_\varepsilon}\right)\frac{\partial \varepsilon}{\partial x_j}\right] + C_{1\varepsilon}\frac{\varepsilon}{k}\left(G_k + C_{3\varepsilon}G_b\right) - C_{2\varepsilon}\rho\frac{\varepsilon^2}{k} + S_\varepsilon \quad (2)$$

The values of constants for the standard k-epsilon model are $C_{1\varepsilon}=1.44$, $C_{2\varepsilon}=1.92$, $C_{\mu}=0.09$, $\sigma_k=1.0$, $\sigma_{\varepsilon}=1.3$.

The realizable k-ε model is a relatively recent development and differs from the standard k-ε model in two important ways : The realizable k-ε model contains a new formulation for the turbulent viscosity and then a new transport equation for the dissipation rate ε has been derived from an exact equation for the transport of the mean square vorticity fluctuation. The transport Equations for the Realizable k-ε model are presented in equations (3) and (4) :

$$\frac{\partial}{\partial t}(\rho k)+\frac{\partial}{\partial x_j}(\rho k u_j)=\frac{\partial}{\partial x_j}\left[\left(\mu+\frac{\mu_t}{\sigma_k}\right)\frac{\partial k}{\partial x_j}\right]+G_k+G_b-\rho\varepsilon-YM+S_k \quad (3)$$

$$\frac{\partial}{\partial t}(\rho \varepsilon)+\frac{\partial}{\partial x_j}(\rho \varepsilon u_j)=\frac{\partial}{\partial x_j}\left[\left(\mu+\frac{\mu_t}{\sigma_{\varepsilon}}\right)\frac{\partial \varepsilon}{\partial x_j}\right]+\rho C_1 S_{\varepsilon}-\rho C_2\frac{\varepsilon^2}{k+\sqrt{\nu\varepsilon}}+C_{1\varepsilon}\frac{\varepsilon}{k}C_{3\varepsilon}Gb+S\varepsilon \quad (4)$$

The values of constants for the realizable k-epsilon are $C_{1\varepsilon}=1.44$, $C_2=1.9$, $\sigma_k=1.0$, $\sigma_{\varepsilon}=1.2$.

The standard k-ω model is an empirical model based on model transport equations for the turbulence kinetic energy (k) and the specific dissipation rate (ω), which can also be thought of as the ratio of ε to k. Production terms have been added to both the k and ω equations, which have improved the accuracy of the model for predicting free shear flows. The transport Equations for the Standard k- ω model are presented in equations (5) and (6) :

$$\frac{\partial}{\partial t}(\rho k)+\frac{\partial}{\partial x_i}(\rho k u_i)=\frac{\partial}{\partial x_j}\left(\Gamma_k\frac{\partial k}{\partial x_j}\right)+G_k-Y_k+S_k \quad (5)$$

$$\frac{\partial}{\partial t}(\rho \omega)+\frac{\partial}{\partial x_i}(\rho \omega u_i)=\frac{\partial}{\partial x_j}\left(\Gamma_{\omega}\frac{\partial \omega}{\partial x_j}\right)+G_{\omega}-Y_{\omega}+S_{\omega} \quad (6)$$

The values of constant for the standard k-omega are $\alpha_{\infty}^{*}=1$, $\alpha_{\infty}=0.52$, $\alpha_0=\frac{1}{9}$, $\beta_{\infty}^{*}=0.09$, $\beta_i=0.072$, $R_{\beta}=8$, $R_k=6$, $R_{\omega}=2.95$, $\varsigma^{*}=1.5$, $M_{t0}=0.25$, $\sigma_k=2.0$, $\sigma_{\omega}=2.0$

The shear-stress transport (SST) k- ω model was developed to effectively blend the robust and accurate formulation of the k-ω model in the near-wall region with the free-stream independence of the k-ε model in the far field. Hence The standard k- ω model and the transformed k-ε model are both multiplied by a blending function and both models are added together. The model includes some refinements i.e. The SST model incorporates a damped cross-diffusion derivative term in the ω equation. The definition of the turbulent viscosity is modified to account for the transport of the turbulent shear stress. The modeling constants are different. Transport Equations for the SST k-ω model are presented in equations (7) and (8) :

$$\frac{\partial}{\partial t}(\rho k)+\frac{\partial}{\partial x_i}(\rho k u_i)=\frac{\partial}{\partial x_j}\left(\Gamma_k\frac{\partial k}{\partial x_j}\right)+\tilde{G}_k-Y_k+S_k \quad (7)$$

$$\frac{\partial}{\partial t}(\rho \omega)+\frac{\partial}{\partial x_i}(\rho \omega u_i)=\frac{\partial}{\partial x_j}\left(\Gamma_{\omega}\frac{\partial \omega}{\partial x_j}\right)+G_{\omega}-Y_{\omega}+D_{\omega}+S_{\omega} \quad (8)$$

The values of constant for the SST k-omega are $\sigma_{k,1}=1.176$, $\sigma_{\omega,1}=2.0$, $\sigma_{k,2}=1.0$, $\sigma_{\omega,2}=1.168$, $\alpha_1=0.31$, $\beta_{i,1}=0.075$, $\beta_{i,2}=0.0828$.

2.1.3 Computation Condition

The thermodynamic properties of air were taken to be at 28 °C under standard atmospheric conditions. Heat generated by heater mat was set at 59 °C, and waves models to move the fluid were in the form of sine and square waves. The details of the properties and the boundary conditions used in this simulation are shown in Table 1.

The iteration was conducted using 1/80 second of time step size. The initial (t = 0) position of the diaphragm was taken to be at the bottom of the cavity. The diaphragm motion was assumed to mimic piston movement within a cylinder, which was expressed in equation (9) for sine wave and equation (10) for square wave.

Table 1 Computation condition

Model Settings		2ddp [a], Unsteady
Fluid		Air
Fluid Properties	Density	1.225 Kg/m^3
	Viscosity	1.7894e^{-05}Kg/ms
	C_p [b]	1006.43 J/kg-k
	k_t [c]	0.0242 w/m-k
Boundary Condition	Membrane 2 & 1	sine and square (UDF[d])
	Pressure Outlet	0 Pascal
	Heater	59 °C
	Frekuensi	80 Hz
	Amplitudo	2 mm/s
	Wave	sine and square
	Flow	turbulent

[a] 2ddp = dimensional double precision
[b] C_p = the heat capacity at constant pressure
[c] k_t = the thermal conductivity
[d] UDF = user defined function

$$V_0=A\sin\ \omega t \quad (9)$$

$$V_0=\left\{\frac{4}{\pi}\sum_{A=1,2,3....}^{\infty}\frac{\sin\ \ 2A-1\ \ \omega t}{2A-1}\right\} \quad (10)$$

where A is the maximum velocity (velocity amplitude) generated by the movement of the diaphragm inside the cavity and t is the operational time. Under these conditions, the unsteady, Reynolds-averaged Navier-Stokes equations within the solution domain were solved along with the energy equation for a range of operating conditions. Movement of the piezoelectric membrane is illustrated as a combined sine and square wave in Figure 2.

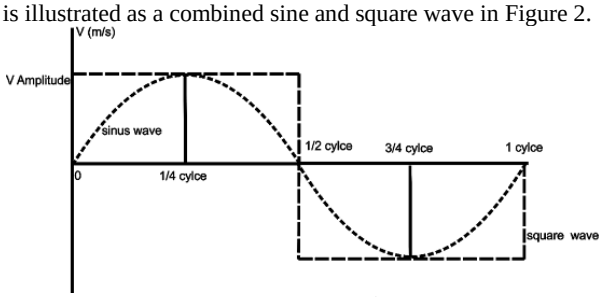

Figure 2 Variation of the wave

2.2 Experimental Setup

Experimental activities was caried out to produce a synthetic jet flow by using two sweep function generators to create sine and square signals . The detail of the experimental setup is shown in Figure 3.

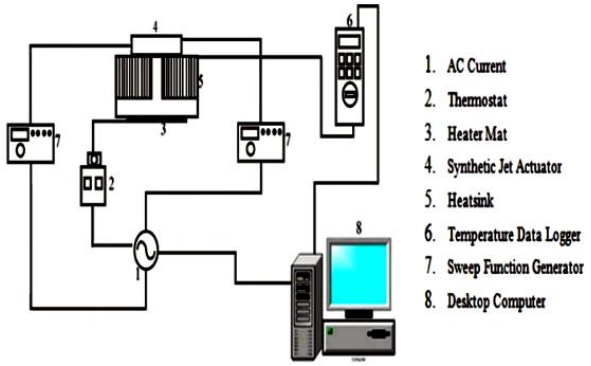

Figure 3 Experimental Setup

Experimental work was carried out by measuring the temperature at the heat sink using thermocouples of K type which were connected to temperature data loggers with measurement accuracy ± 0.05 ^{o}C. The heat sink used for the experiment had a circular form with 32 fins, 11 cm of diameter and 5 cm of height. The heat sink was made of cylindrical aluminum which was shaped by using material removal methods. Heat source was obtained from the heater mat placed at the bottom of the heat sink, and it was set to 59 ^{o}C using a thermostat. Measurements were performed under open conditions at ambient temperature of 28 ^{o}C. More than 3600 individual data were recorded for each measurement run which give estimated statistical uncertainty of 1%.

The synthetic jets actuator used in this study were constructed in the form of a symmetric cylinder cavity with membranes at the top and bottom. The membranes pushed the air inside the cavity to escape into the surrounding air through exit nozzles. The casing body of synthetic jet actuator was made of nylon material because it was easy to shape and has a good insulator properties. Figure 4 shows the synthetic jet actuator bottom area which has 20 channels of flow passage. The distance between the channel was 9 mm and the channel diameter was 2 mm. The sine and square waves forcing to the membranes were generated by two sweep function generators with the frequency of 80 Hz, 120 Hz and 160 Hz using maximum signal setting at 28.8 Volt.

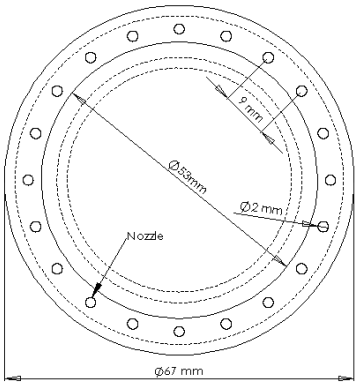

Figure 4 Synthetic jet actuator bottom view

3.0 RESULTS AND DISCUSSION

3.1 Turbulent Intensity

Figure 5(a) to 5(d) describe the contours of turbulence intensity generated by the computational simulation using standard k-epsilon, realizable k-epsilon, standard k-omega and k-omega SST (Shear Stress Transport) respectively. The figure shows representative results for the excitation of sine and square signals with a frequency of 80 Hz and amplitude 0.002 m/s.

From figure 5(a) the maximum value of turbulent intensity is located in the nozzle for about 3.69 % with in 1/2 cycle periode, and then figure 5(b) indicates that the maximum value of turbulent intensity is located in the cavity of synthetic jet for about 8.80 % at oscillation periode of 1/4 cycle. Further Figure 5(c) suggests that the maximum value of turbulent intensity is located in the nozzle for about 5.71 % at oscillation periode of 1 cycle. Then figure 5(d) the maximum value turbulent intensity located in the area nozzle at value 1.93 % on periode oscillation of1 cyle.

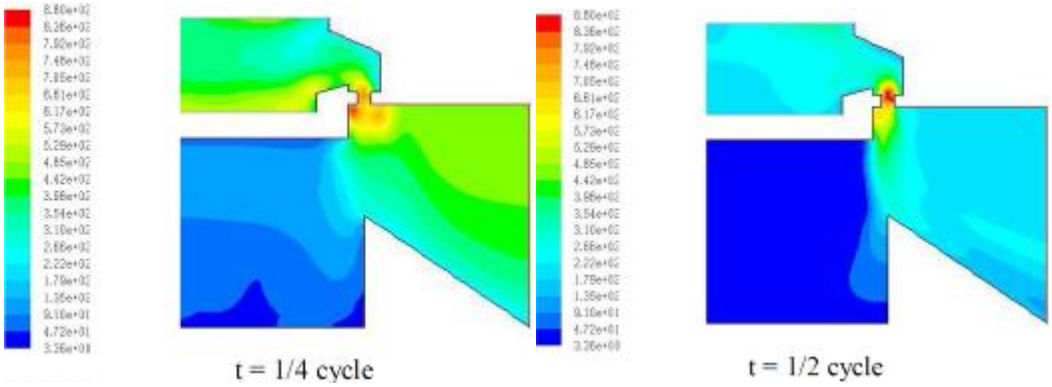

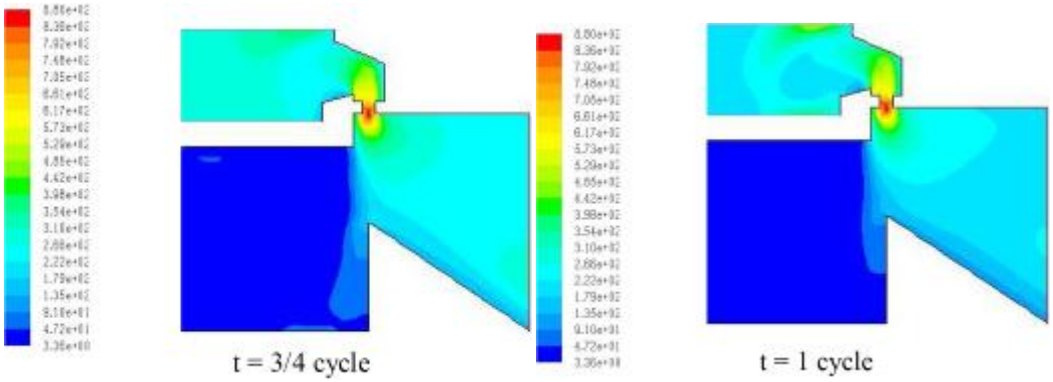

(a) standard k-epsilon under combined wave excitation

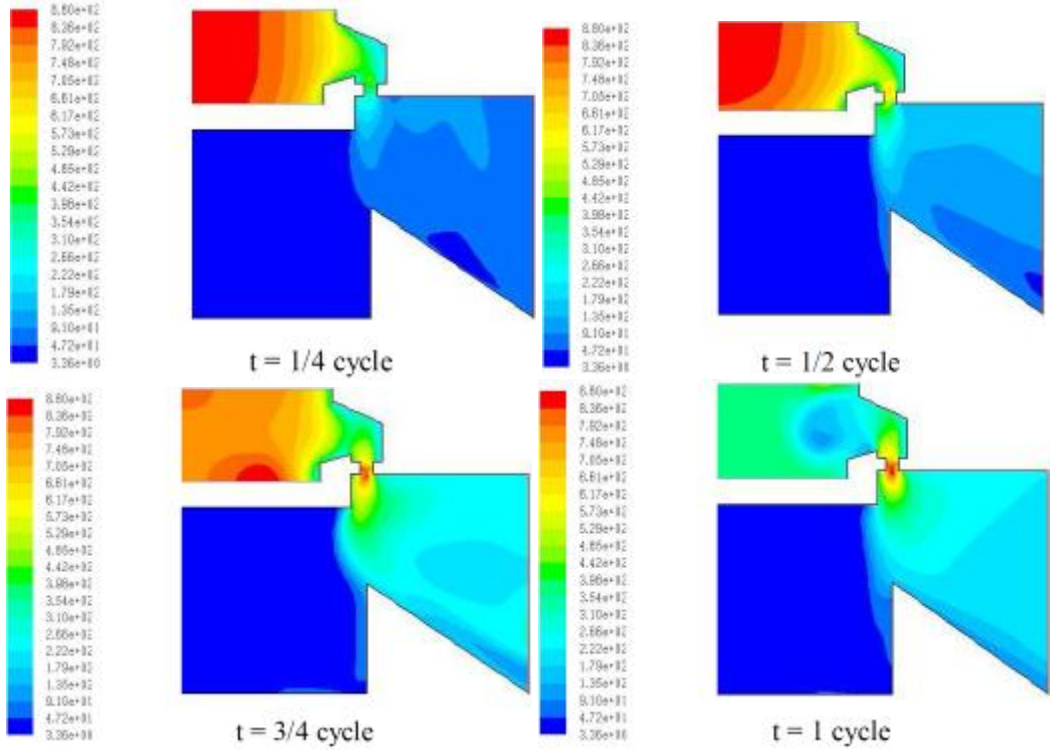

(b) realizable k-epsilon under combined wave excitation

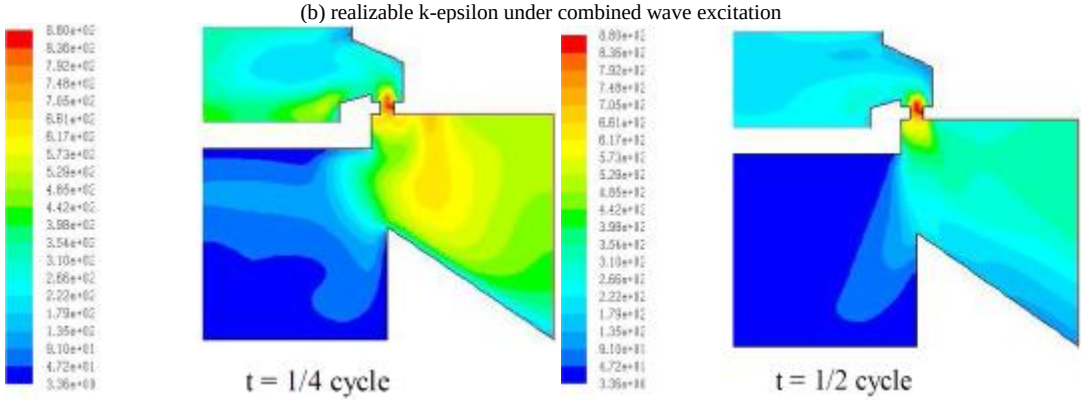

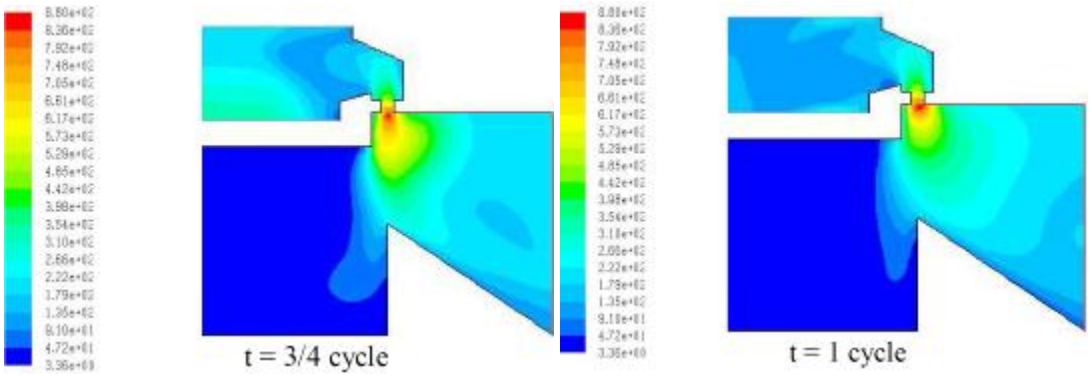

(c) standard k-omega under combined wave excitation

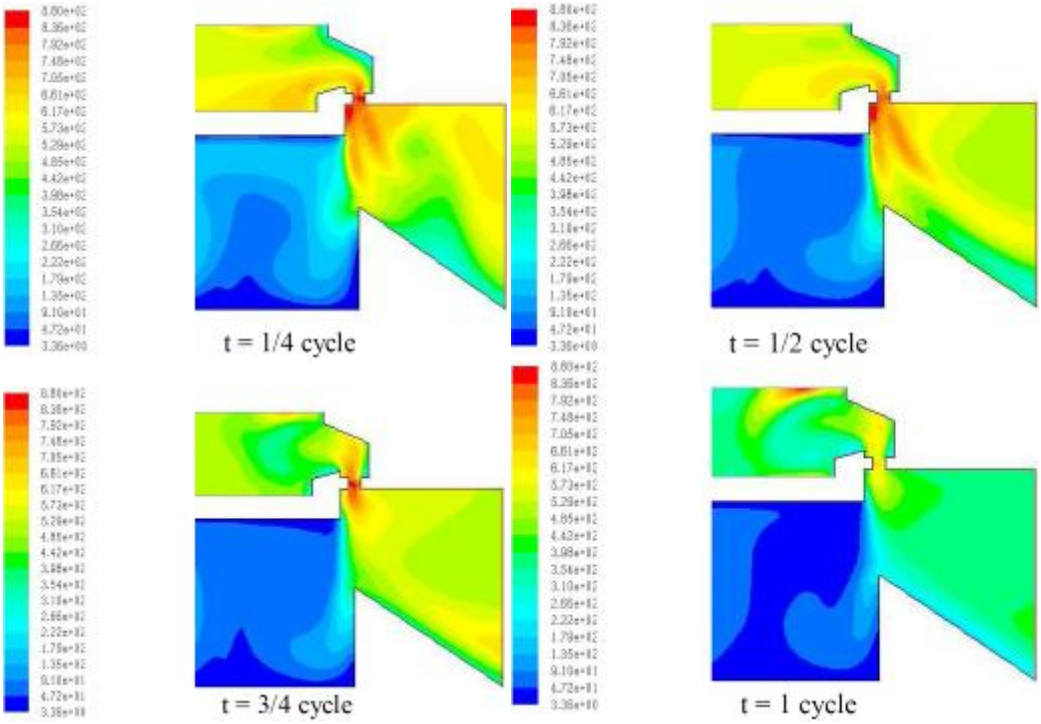

(d) k-omega SST under combined wave excitation

Figure 5 Turbulent Intensity contour (%)

3.2 Static Temperature

Figure 6 (a) to (d) describe the contours of static temperature generated by the computational simulation using standard k-epsilon, realizable k-epsilon, standard k-omega and k-omega SST (Shear Stress Transport) respectively. The figure shows representative results for the excitation of sine and square signals with a frequency of 80 Hz and amplitude 0.002 m/s.

These contours indicate the temperature condition inside and outside the cavity along the heat sink. Apparent temperature changes can be seen in each period. In the period of 1 cycle a mixing occurs from the heat sink into the synthetic jet cavity. It seems that the air flow imposes an obstruction effect to the membrane so that it does not have sufficient power to push the air out. Hence, instead of blowing low temperature air, the synthetic jet actuator discharges heated air which is drawn back to the cavity at the previous suction phase.

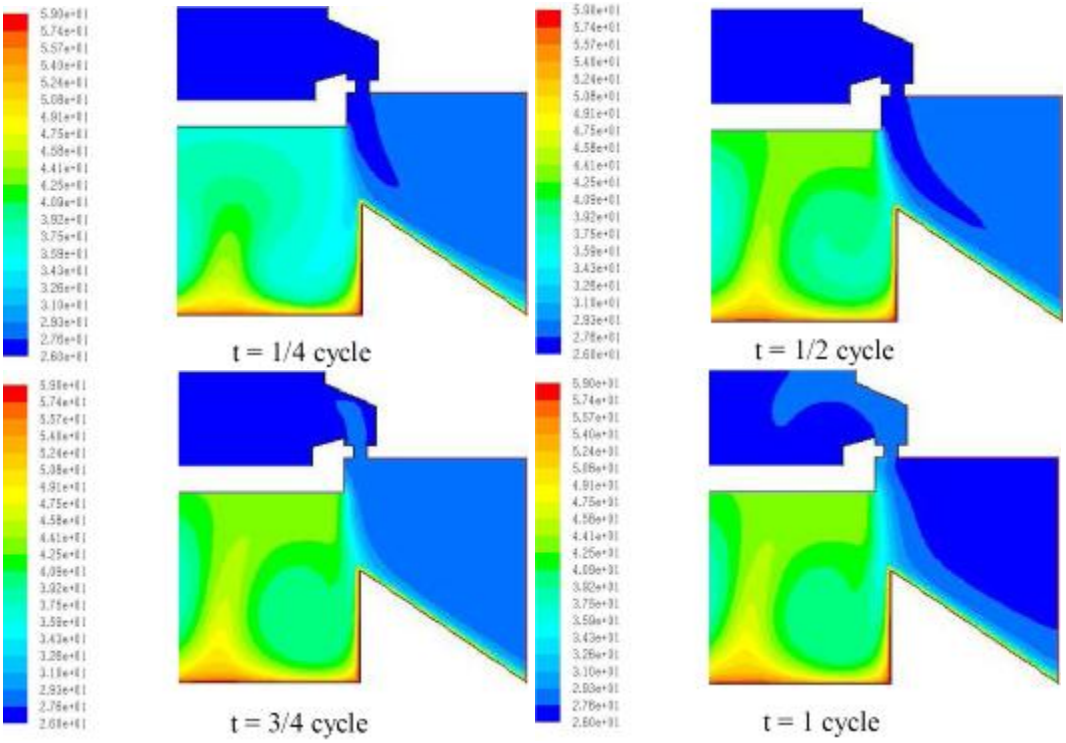

(a) standard k-epsilon under combined wave excitation

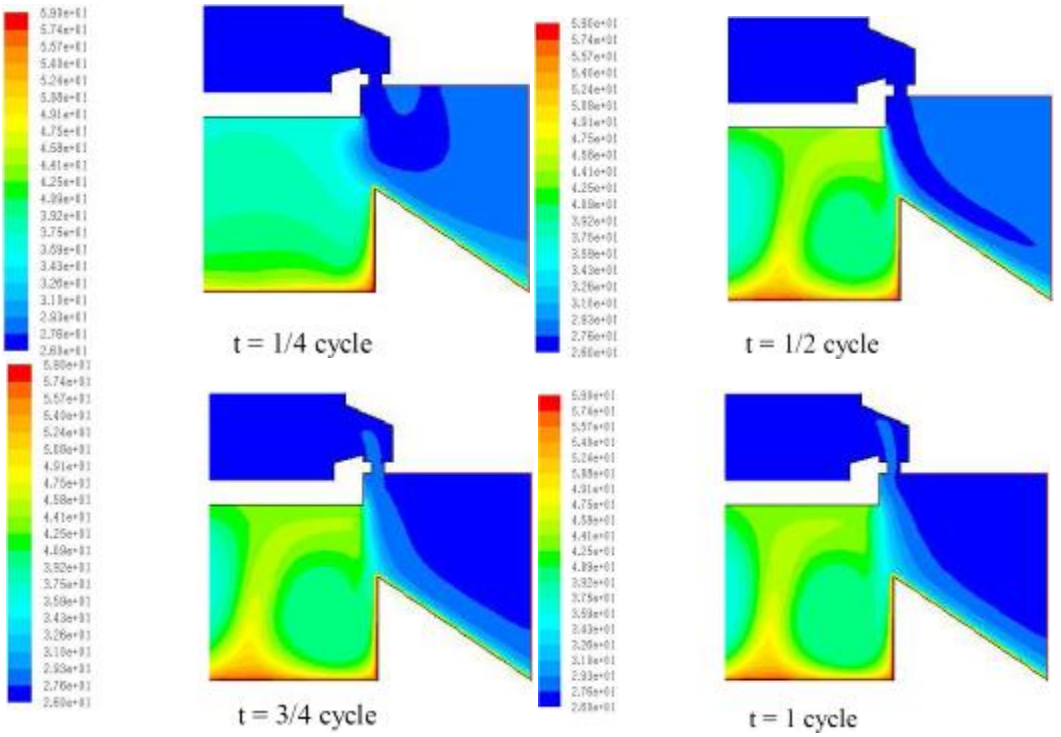

(b) realizable k-epsilon under combined wave excitation

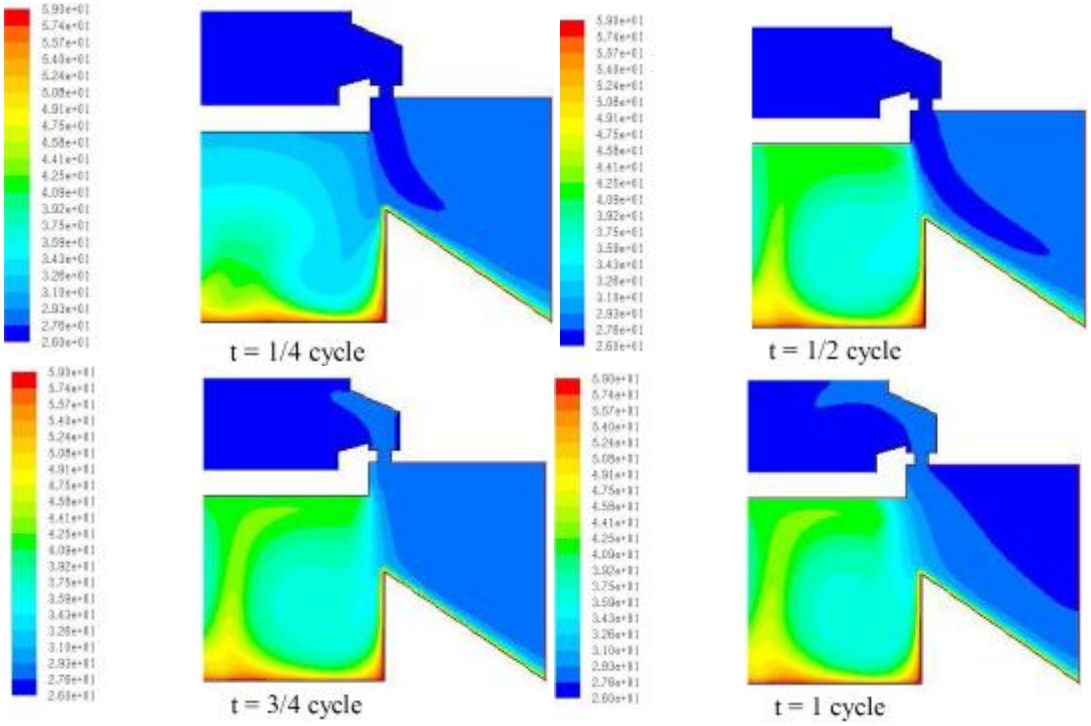

(c) standard k-omega under combined wave excitation

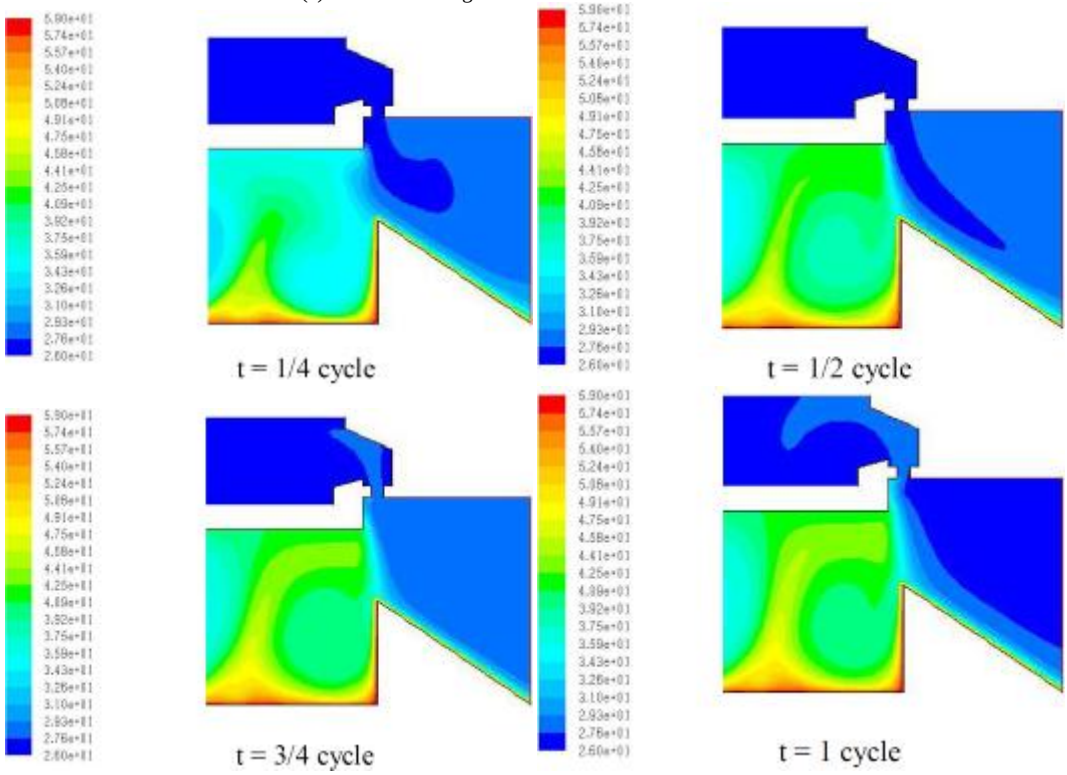

(d) k-omega SST under combined wave excitation

Figure 6 Static Temperature (^{0}C)

3.3 Vector Plots

Figure 7 (a) to 7 (d) describe the velocity vectors plot generated by the computational simulation using standard k-epsilon, realizable k-epsilon, standard k-omega and k-omega SST (Shear Stress Transport) respectively. The figure shows representative results for the excitation of sine and square signals with a frequency of 80 Hz and amplitude 0.002 m/s.

At 1/4 cycle and 1/2 cycle it can be seen that air flow is blown into the heat sink, and then at 3/4 cycle and 1 cycle the suction flow occurs that brings air into the cavity of synthetic jet. This periodical movement causes the mixing of heat from the heat sink into the synthetic jet cavity.

From all the above results and discussions, it can be revealed that despite a slight difference in the absolute value of flow and thermal field quantities, all turbulence models applied

in the simulation give similar tendencies to the characteristics of thermal flow field in the current flow configuration.

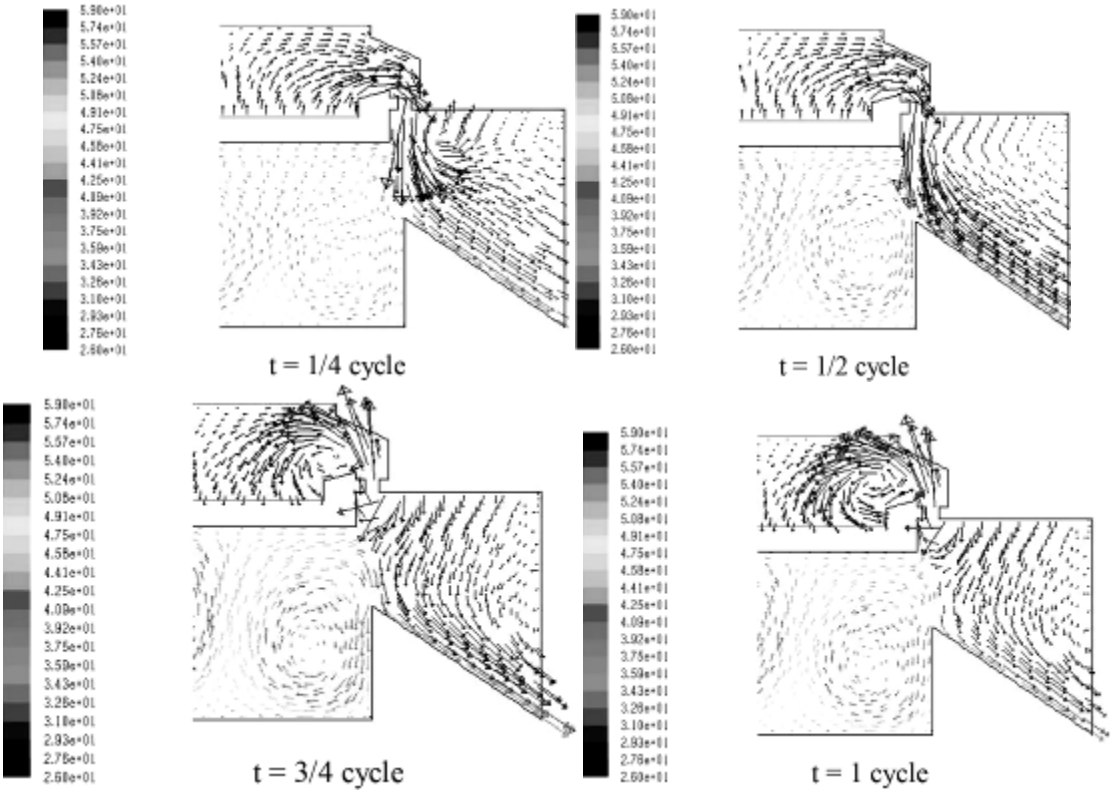

(a) standard k-epsilon under combined wave excitation

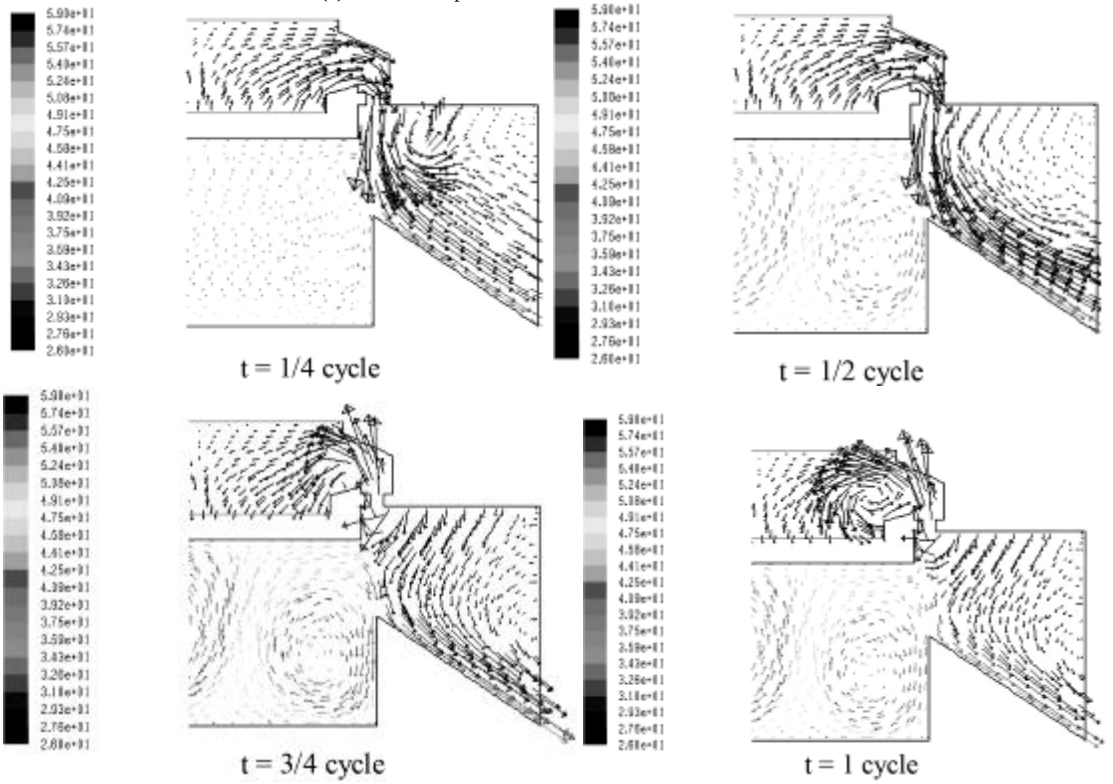

(b) realizable k-epsilon under combined wave excitation

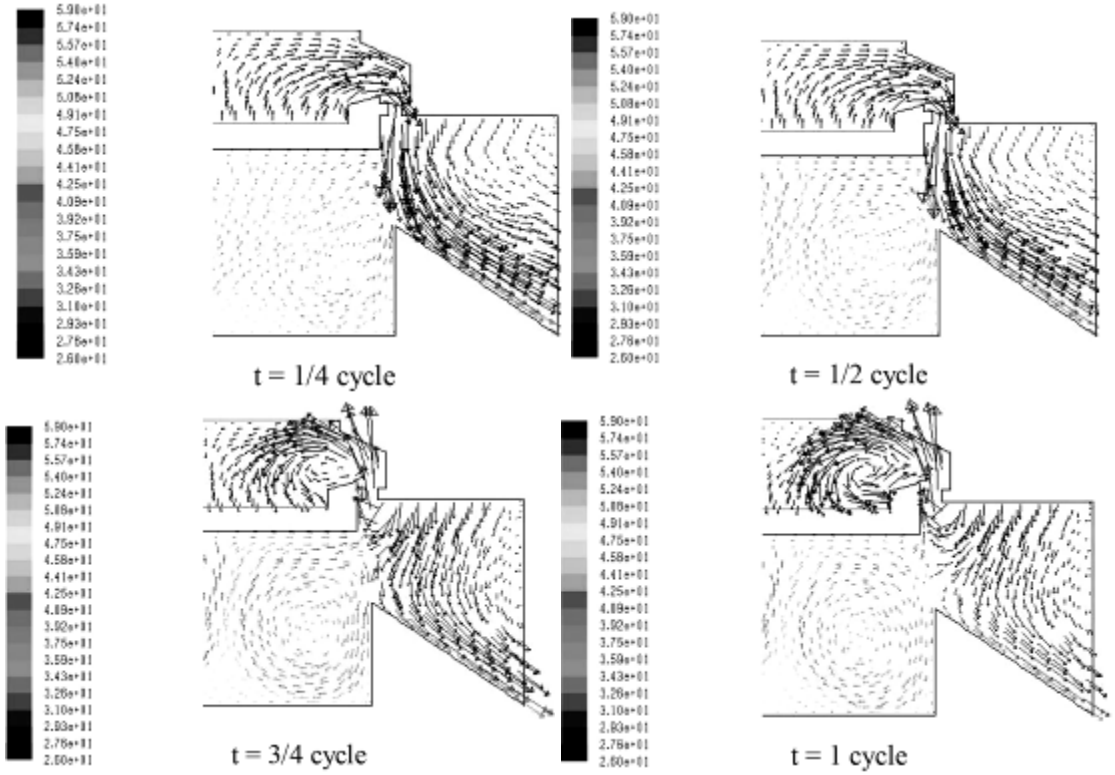

(c) standard k-omega under combined wave excitation

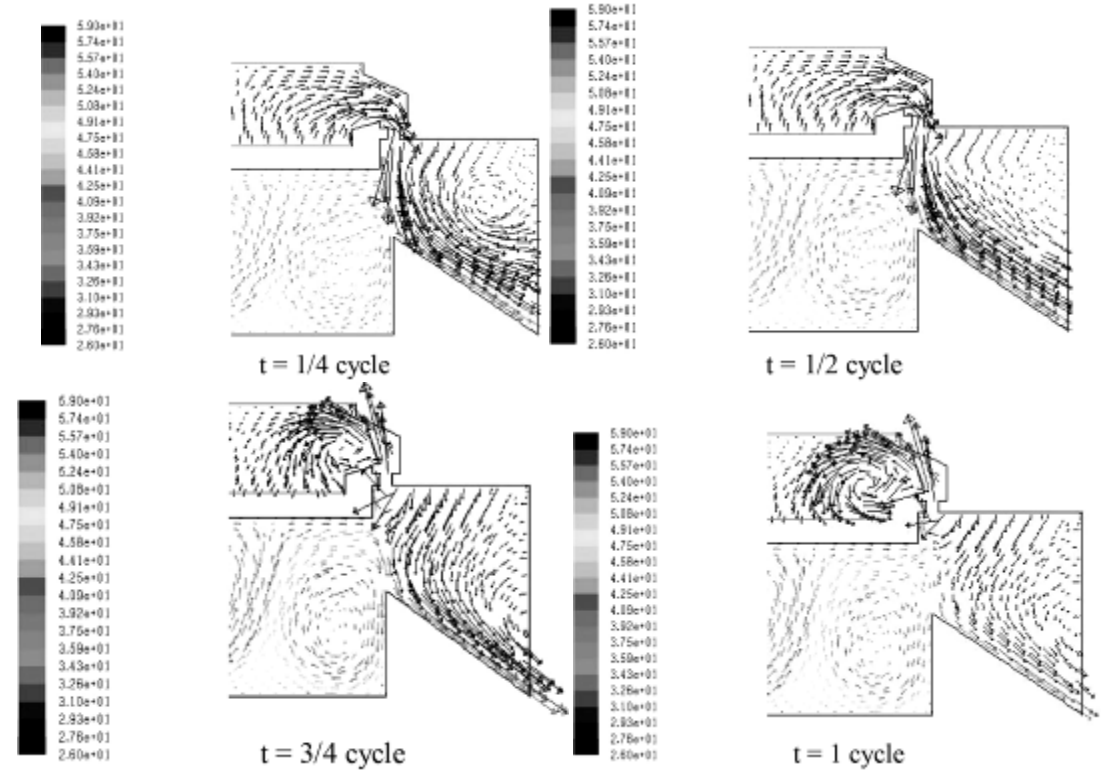

(d) k-omega SST under combined wave excitation

Figure 7 Vector plot

3.4 Experimental Work

The measurement results of heat sink temperature obtained in an open space conditions within time period of 60 minutes are described in Figure. 8 under combined wave excitation. It is clear that the combined wave excitation and frequency plays important roles in synthetic jet cooling in both forcing modes of current study. The figure suggests that the best combined wave excitation for cooling is achieved at sine 80 Hz and square 120 Hz indicated by the temperature of the heat sink which decrease steadily as time progress. Meanwhile the combined forcing wave of sine 80 Hz and square 80 Hz obtained the minimum

temperature of the heat sink for about 57.5 ^{o}C at 20 minutes but then the temperature of heat sink increases. Furthermore a similar trend can also be observed for combined excitation wave at sine 80 Hz and square 160 Hz which obtain the minimum temperature of the heat sink for about 57.6 ^{o}C at 30 minutes but the temperature of heat sink increases afterward.

Based of the measured temperature, the heat trasfer coefficient can be evaluated by considering the natural convection effect, the heat energy balance can be evaluated as follow :

$$Q_{i,h} = Q_{o,sj} + Q_{o,nc} \quad (11)$$

where $Q_{i,h}$ is the heat generated by the heater that is conducted through the heat sink, $Q_{o,sj}$ is the heat removed by the synthetic jet effect, and $Q_{o,nc}$ is the heat removed by natural convection effect. The heat trasfer coefficient of the synthetic jet h_{sj} can be evaluated as follow:

$$h_{sj}A_{sj}\left(\frac{dT}{dt}\right) = Q_{i,h} - h_{nc}A_{nc}\left(\frac{dT}{dt}\right) \quad 12$$

Where A_{sj} is the synthetic jet effective cooling area, (dT/dt) is the rate of temperature change measured in the experiment, h_{nc} is the value of the air heat transfer coefficient with the custom heatsink, and A_{nc} is the cooling area affected by the air natural convection. Applying equations (11) and (12), the calculation results of heat transfer coefficient for sine and square signals are shown in Figure 9. The figure describes the time history of heat transfer coefficient during time period of 60 minutes.

From Figure 9 it can be observed that the highest heat transfer coefficient is reached by the combined excitation at sine 80 Hz and square 80 Hz with maximum value at 20 minutes. After that, the heat transfer coefficient will dropped significantly. The figure also indicates that after some period of creating cooling effect to the heat sink, the synthetic air jet creates opposite effect of imposing heating to the heat sink. Meanwhile for the case of combined excitation at sine 80 Hz and square 120 Hz the heat transfer coefficient increases steadily, even until 60 minutes. The above results indicate that for a heat removal the sine 80 Hz and square 120 Hz forcing is more effective than the other combination. However, the current results of obtained heat transfer coefficients are still below those reported by Jing Zhou *et al*. (2007). They report a maximum value heat transfer coefficient of 95 W/m^{2}K, meanwhile in this study the maximum heat transfer coefficient achieved is 22 W/m^{2}K.

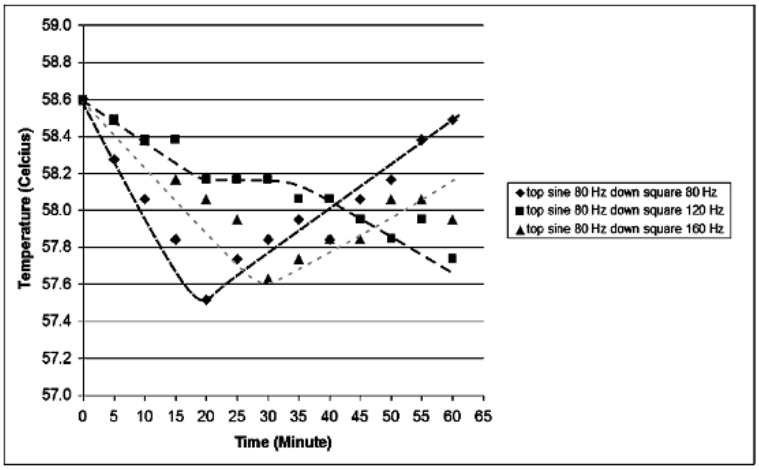

Figure 8 Time history of heat sink temperature under synthetic jet suction and blowing with sine and square wave forcing

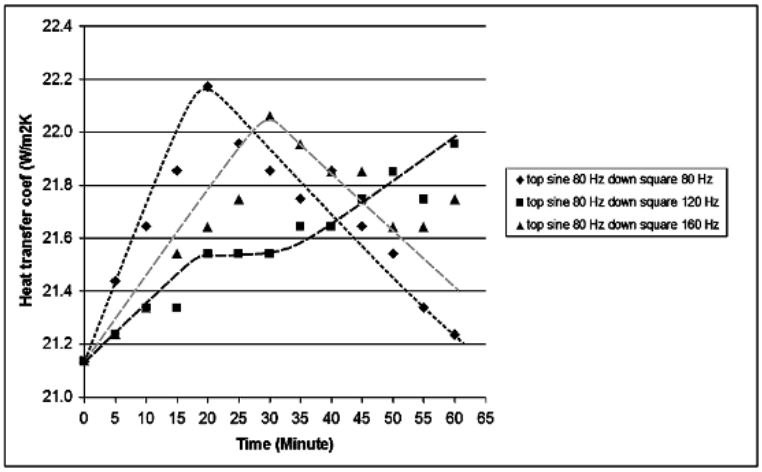

Figure 9 Heat transfer coefficient graphic to tim

4.0 CONCLUSION

An investigation on the flow and heat transfer characteristics of original designed synthetic jet prototypes has been done in an impinging flow configuration under combination of excitation wave. The study combining computational and experimental method on the synthetic jet actuator oscillation has been comprehensively conducted using sine and square waveform excitation. The oscillation frequency in synthetic jet which describes the number of suction and discharge stroke in a second of the membrane in the cavity obviously plays important role in the heat transfer process.

Despite a slight difference in the absolute value of flow and thermal field quantities, all turbulence models applied in the simulation give similar tendencies to the characteristics of thermal flow field in the current flow configuration. The combined excitation using sine 80 Hz and square 120 Hz is more effective than the other combinations, because it is able to decrease the temperature in a longer time period. Current achievements of the work suggest some design consideration to make a compact synthetic jet actuator with high cooling efficiency i.e. by varying synthetic jet distance to the impinging surface of the heat sink. This is done to provide an air exchange heat from the heat sink to the air environment.

Acknowledgement

The authors would like to thank the DRPM University of Indonesia , for funding this research through Research with number contract No. 1927/H2.R12.1/HKP.05.00/2012.

References

[1] Harinaldi, Rhakasywi, D., Defriadi, R. 2011. Flow and Heat Transfer Characteristics of an Impinging Synthetic Air Jet under Sinusoidal and Triangular Wave Forcing. *IJET-IJENS*. 11(03): 29–36.

[2] Chaudhari, M., Puranik, B., Agrawal, B. 2009. Heat Transfer Characteristics of Synthetic Jet Impingement Cooling. *International Journal Of Heat And Mass Transfer*. In Press. doi:10.1016/j.ijheatmasstransfer.11.005.

[3] Pavlova, A., Amitay, M. 2006. Electronic Cooling Using Synthetic Jet Impingement. *Journal of Heat Transfer*. 128(9): 897–907.

[4] Gulati, P., Katti, S., Prabhu, V. 2009. Influence of the Shape of the Nozzle on Local Heat Transfer Distribution Between Smooth Flat Surface and Impinging Air Jet. *International Journal of Thermal Sciences*. 48(3): 602–617.

[5] Amitay, M., Pavlova, A., 2006. Electronic cooling with synthetic jet impingement. *Journal of Heat Transfer*. 128: 897–907.

[6] Chaudhari, M., Puranik, B., Agrawal, A. 2010. Heat Transfer Analysis in a Rectangular Duct Without and with Cross-Flow and an Impinging Synthetic Jet. IEEE Transaction on Component and Packaging Technologies. 33(2).

[7] Mahalingam, R., Glezer, A. 2005. Design and Thermal Characteristics of a Synthetic Jet Ejector Heat Sink. *Journal of Electronic Packaging*. 127: 172–177.

[8] Chaudhari, M., Puranik, B., Agrawal, A. 2010. Effect of Orifice Shape in Synthetic Jet-Based Impingement Cooling. Experimental Thermal Fluid Sci. 34(2): 246–256.

[9] Lee, D.H., Song, J., Myeong, C.J., 2004. The effect of nozzle diameter on impinging jet heat transfer and fluid flow. Journal . Heat Transfer 126, pp. 554–557.

[10] Beitelmal, A. H., Shah, A. J., Saad, M. A. 2006. Analysis of an Impinging Two Dimensional Jet. *Journal. Heat Transfer*. 128: 307–310.

[11] Lienhard, J. H., 2006. Heat Transfer by Impingement of Circular Free-Surface Liquid Jets. In: 18th National and 7th ISHMT – ASME Heat and Mass Transfer Conference.

[12] Lee, J., Lee, S.J. 2000. The Effect of Nozzle Configuration on Stagnation Region Heat Transfer Enhancement of Axisymmetric Jet Impingement. *International Journal Heat Mass Transfer*. 43: 3497–3509.

[13] Tsubokura, M., Kobayashi, N., Taniguchi, N. 2002. Numerical Study on the Difference of the Eddy Structures Between Plane and Round Impinging Jets. In: Proceedings of the 5th International Symposium on Engineering Turbulence Modelling and Measurements, Mallorca, Spain.

[14] Poh, H. J., Kumar, K., Mujumdar, A. S. 2005. Heat Transfer from a Pulsed Laminar Impinging Jet. International. *Commun. Heat Mass Transfer*. 32(10): 1317– 1324.

[15] Kercher, D. S., Lee, J. B., Brand, O., Allen, M.G., Glezer, A. 2003. Microjet Cooling Devices for Thermal Management of Electronics. *IEEE Transaction on Components and Packaging Technologies*. 26(2): 359–366.

[16] Harinaldi., Rhakasywi, D., Defriadi, R. 2011. Computational Study of Triangular Waveform Oscillation Mode to The Temperature Distribution of a Heated Wall Impinged by a Synthetic Jet. IMAT 4th - Melaka, Malaysia.

[17] Zhou, Z. J., Ming, T. X. 2007. Experimental Study on Flow and Heat Transfer Characteristics of Synthetic Jet Driven by Piezoelectric Actuator. *Springerlink*. 50(2): 221–229.